

Mg-M-LiH Alloys Prepared by Mechanical Milling and their Hydrogen Storage Characteristics

K. Suárez-Alcántara^{1*}, A.F. Palacios-Lazcano², T. Funatsu³, J. G. Cabañas-Moreno⁴

¹ UNAM-IIM Morelia, Antigua carretera a Pátzcuaro 8710, Col. Ex-hacienda de San José de la Huerta, Morelia, Michoacán, 58190, México.

² ESIME Zacatenco, Av. Luis Enrique Erro S/N, Unidad Profesional Adolfo López Mateos, Zacatenco, Delegación Gustavo A. Madero, Distrito Federal, 07738, México.

³ Techno System CO., LTD, Karasakinaka 3-1-1, Takatsuki-City, Osaka, Japan.

⁴ Centro de Investigación y de Estudios Avanzados, IPN, Av. Instituto Politécnico Nacional 2508, México, D. F., 07360, México.

ABSTRACT

Mg₉₆M₂(LiH)₂ (M=Y, Zn, Al, Ag), Mg₉₈(LiH)₂ and Mg₉₆(LiH)₄ powder alloys were produced by ball milling and deliberately air-exposed by 12 hours in order to investigate their hydrogen storage properties. The addition of LiH at the level of 2 mol % had a beneficial effect on the kinetics of the hydriding and dehydriding processes at 300 and 350 °C compared to mechanically milled Mg powders. However, the additions of Al, Ag, Zn and Y had an opposite effect on the hydriding/ dehydriding kinetics. The addition of aluminum provided a small advantage in the capacity of hydrogen storage among the tested materials.

Keywords: Hydrogen storage, Mg-M-LiH alloys, magnesium hydride, mechanical alloying



1. Introduction

Magnesium is the archetypical material for hydrogen storage due to its high theoretical gravimetric hydrogen density of 7.6 wt.%. However, the main drawback of pure Mg/MgH₂ as a potential hydrogen storage material is the high temperature required for the dehydriding reaction, i.e., its high thermodynamic stability [1, 2]. This drawback severely limits the possibility of use in mobile applications; nevertheless, stationary applications for high temperature fuel cells or heat storage are still feasible [3]. Even more, 2LiH+Mg/ 2Li+MgH₂ (and the transition metal-doped system) have potential application as negative electrode in rechargeable batteries [4, 5]. A second challenge is to obtain adequate hydriding and dehydriding kinetics. The beneficial influence of ball milling of Mg or MgH₂ is well known in this respect [6, 7, 8]; but still, the dehydriding kinetics are not considered sufficiently adequate. Theoretical and experimental results support the use of different transition metals in order to improve the kinetics and thermodynamics of hydriding/ dehydriding reactions [9, 10, 11, 12, 13, 14, 15, 16, 17, 18, 19]. All together, these effects can be explained by the refinement of particle size and microstructure, increases in surface area, generation of crystalline defects on the surfaces and in the bulk, and the catalytic action of alloying metals or oxides, etc.

In a previous work it has been observed that addition of small quantities of Zn, Al or Ag to Mg during ball milling improves the hydriding kinetics [20]. In the present work, we report the results of synthesizing and testing Mg₉₈M₂(LiH)₂ (M = Y, Zn, Al, Ag) alloys, particularly in terms of the quantity of stored hydrogen and the kinetics of the hydriding/ dehydriding process. Also, we analyze the effects of air-exposed Mg alloys as a way to reduce the costs of production, storage and handling in high-purity Argon protective atmosphere. It must be considered that H₂ as fuel can be produced from different raw materials such as water, biomass, catalytic reforming of methane, etc. where the high purity and homogeneity cannot always be guarantee. Also accidental air-exposure of materials during handling or operation is possible. Thus fabrication, processing and testing of our “traditional” materials under more purity-relaxed oxygen conditions must be done if extensive use of hydrogen storage materials is intended.

2. Experimental

2.1 Production of the Powder Alloys

Mg₉₆M₂(LiH)₂ (M= Al, Ag, Zn, Y), Mg₉₈(LiH)₂ and Mg₉₆(LiH)₄ powder alloys were prepared by mechanical milling. The corresponding molar quantities of elemental powders of Mg, Al, Ag, Zn, Y (99.8 % purity, particle size < 45 µm) and LiH (99.9 % purity, particle size < 3 µm) were used as received from Aldrich. The addition of LiH, in lieu of metallic Li, was considered a better approach to ensure the retention of Li in the final, as-milled powder mixtures. The mixtures were prepared in a Fritsch Pulverisette, model 6, milling device, at 350 rpm. The total effective milling time was 60 hours in cycles of 1.5 hours of milling and 0.5 hours of pause. The ball-to-powder ratio was 11:1. The milling vial container (500 ml capacity) and the 50 balls of 1 cm diameter and 4 balls of 2 cm diameter were made of chromium steel. In total, 30 grams of the powders plus 3 ml of methanol (as milling control agent) were charged in the container and sealed under Argon atmosphere.

After milling, the container was cooled to room temperature and the powders were gradually exposed to air for 12 hours. Afterwards, these milled and passivated powders were kept in Ar-filled glass vials.



Subsequently, all handling for characterization was performed at open-air atmosphere. Pure Mg was given the same milling treatment, to be used as a reference and presented whenever needed below.

2.2 Hydriding and dehydriding reactions

Hydrogen storage properties were determined by means of a PCTM-6000 (Techno System Co., LTD) gravimetric equipment operating under chromatographically-pure hydrogen atmosphere. The equipment was carefully calibrated for pressure and temperature effects on the sample holder buoyancy. The alloys were subjected to hydriding and dehydriding activation cycles, before Pressure – Composition Isotherms (PCI) were determined. The activation cycles started with sample annealing at 350°C under dynamic vacuum for 30 minutes. Then, the samples were subject to consecutive hydriding and dehydriding cycles at 350°C. For the hydriding experiments, the hydrogen pressure was increased from 0.1 bar to 30 bar in steady pressure steps, the pressure increase ramp being performed in 25 minutes. The dehydriding process was carried out by reversing these conditions; the pressure decrease ramp was performed in 25 minutes. A single hydriding/dehydriding cycle took 6 hours.

In the PCI determination, the hydrogen pressure increase/decrease steps in PCI measurements were 0.1 bar in the 0.1-1 bar interval and 1 bar in the 1-30 bar interval. The PCI measurement was performed in a total time of 16 hours. After that, the temperature was fixed at 300°C and a hydriding/ dehydriding cycle was performed on the same sample. Finally, alloys were heated again at 350°C and exposed to hydrogen at 30 bar for 3 hours for further X-ray diffraction and scanning electron microscopy characterization of the hydrided powders.

2.3 Powder X-ray diffraction

X-ray diffraction (XRD) patterns were taken on a D-500 diffractometer (SIEMENS) using monochromatic $\text{CuK}\alpha 1$ ($\lambda = 1.54056\text{\AA}$) radiation. A scanning range from 15° to 80° was used with steps of 0.03° and 5 s per step. XRD patterns were taken without any atmosphere-protective layer, the samples being flat pressed in the sample holder. The MUAD software was used for XRD data processing [21].

2.4 Scanning electron microscope

The as-milled and hydrided alloys were observed in a XL/SFEG/SIRION SEM microscope (FEI Company) at 5 and 15 kV. A few milligrams of sample were attached to a carbon tape and transferred to the microscope chamber. All handling was performed in open air.

3. Results

3.1 XRD and SEM Characterization of as-Milled Powders

XRD patterns of as milled powders are shown in Figure 1. The diffraction peaks corresponding to magnesium, the major component, were clearly defined. Minor Fe contamination from the milling operation produced a small peak at about 44.5° in 2 θ ; Rietveld refinements (and EDS analysis, see below) account for less than 2 wt. % of Fe. The slight shifts in Mg peaks positions indicate a small distortion in cell lattice compared to the values found for as-milled pure Mg (Table I, Mg ICSD-642651). These distortions can be attributed to alloying effects. The addition of LiH produced minor distortions in the Mg lattice in $\text{Mg}_{98}(\text{LiH})_2$ and $\text{Mg}_{96}(\text{LiH})_4$, as indicated in Table 1. A noticeable lattice contraction was observed in $\text{Mg}_{96}\text{Al}_2(\text{LiH})_2$, probably due to the smaller atomic size and larger valency of Al compared to



Mg. The $\text{Mg}_{96}\text{Al}_2(\text{LiH})_2$ mixture presented the larger contraction in the Mg lattice among the tested materials. Lattice contraction was also observed in $\text{Mg}_{96}\text{Ag}_2(\text{LiH})_2$ and $\text{Mg}_{96}\text{Zn}_2(\text{LiH})_2$, but to a lesser extent compared to $\text{Mg}_{96}\text{Al}_2(\text{LiH})_2$. In the $\text{Mg}_{96}\text{Y}_2(\text{LiH})_2$ powder mixture, the unit cell contraction was only detected in the “c” axis. Table I collects the refined Mg cell lattice parameters calculated for our materials.

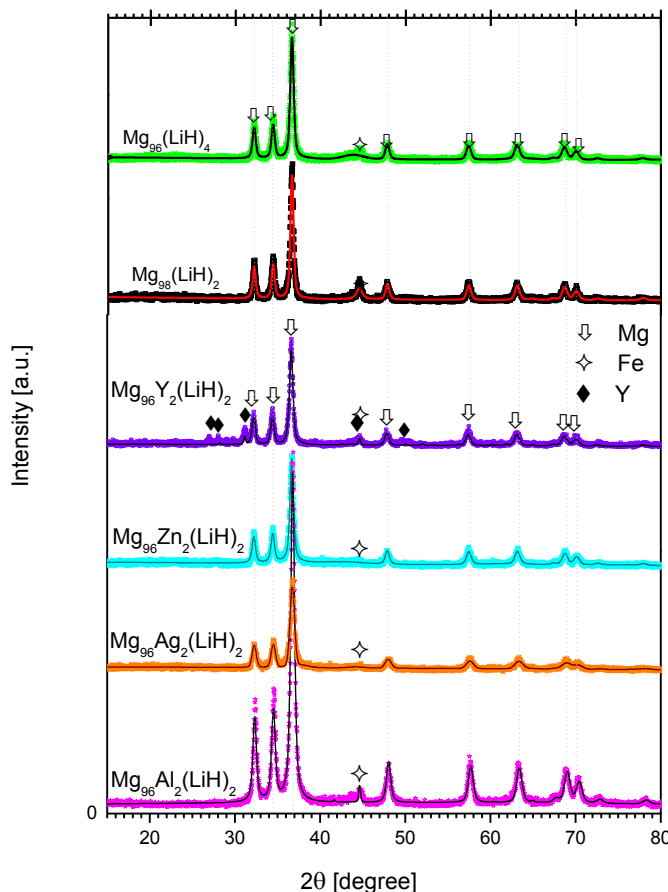


Figure 1. XRD patterns of as-milled and air-exposed powders. Dots: experimental patterns. Line: refined patterns.

Table I. Unit Cell parameters and crystallite size of as-milled materials estimated from XRD refinement.

As-Milled Material	Mg unit cell [Å] ICSD-642651 a=b=3.2094 Å c=5.2108 Å	Mg crystallite size [nm]
--------------------	---	--------------------------



Mg	$a=b=3.2096 \pm 2 \times 10^{-4} \text{ \AA}$ $c=5.2129 \pm 5 \times 10^{-4} \text{ \AA}$	36.4 ± 3.9
Mg ₉₈ (LiH) ₂	$a=b=3.2114 \pm 4 \times 10^{-4} \text{ \AA}$ $c=5.2126 \pm 8 \times 10^{-4} \text{ \AA}$	37.4 ± 1.0
Mg ₉₆ (LiH) ₄	$a=b=3.2090 \pm 2 \times 10^{-4} \text{ \AA}$ $c=5.2084 \pm 6 \times 10^{-4} \text{ \AA}$	40.2 ± 0.6
Mg ₉₆ Al ₂ (LiH) ₂	$a=b=3.1949 \pm 2 \times 10^{-4} \text{ \AA}$ $c=5.1904 \pm 5 \times 10^{-4} \text{ \AA}$	27.8 ± 0.3
Mg ₉₆ Ag ₂ (LiH) ₂	$a=b=3.2002 \pm 5 \times 10^{-4} \text{ \AA}$ $c=5.1927 \pm 9 \times 10^{-4} \text{ \AA}$	97.7 ± 14.3
Mg ₉₆ Zn ₂ (LiH) ₂	$a=b=3.2080 \pm 5 \times 10^{-4} \text{ \AA}$ $c=5.2080 \pm 9 \times 10^{-4} \text{ \AA}$	30.4 ± 0.3
Mg ₉₆ Y ₂ (LiH) ₂	$a=b=3.2097 \pm 5 \times 10^{-4} \text{ \AA}$ $c=5.2093 \pm 9 \times 10^{-4} \text{ \AA}$	33.3 ± 0.8

Mg crystallite sizes estimated by means of the Rietveld refinement of the X-ray patterns of the as-milled materials are also collected in Table I. The data reveal that ball milled Mg₉₆Al₂(LiH)₂, Mg₉₆Zn₂(LiH)₂ and Mg₉₆Y₂(LiH)₂ had crystallite sizes of about 30 nm; i.e., a slight reduction from the ~35-40 nm of pure Mg, Mg₉₈(LiH)₂ and Mg₉₆(LiH)₄ powders. The calculated value for Mg₉₆Ag₂(LiH)₂ was significantly different from all other samples, presenting a crystallite size of about 100 nm.

Despite the affinity of Mg for oxygen and the exposure of the as-milled powders to air at the time of removing them from the milling vial, no clear indication for the formation of crystalline MgO is found in the XRD patterns of Fig. 1. We will come back to this point in the Discussion section.

The as-milled powders were extensively agglomerated. The agglomerate size shows a wide dispersion, as illustrated on the SEM micrograph displayed in Fig. 2 (see supplementary file for more SEM pictures of all materials). Most agglomerates possess sizes in the interval of 1 - 10 µm. Nevertheless, individual particles can be observed with sizes clearly below 1 µm. In many instances, the SEM images provide evidence for the occurrence of cold-welding among small particles during milling, as the mechanism of formation of the agglomerates.



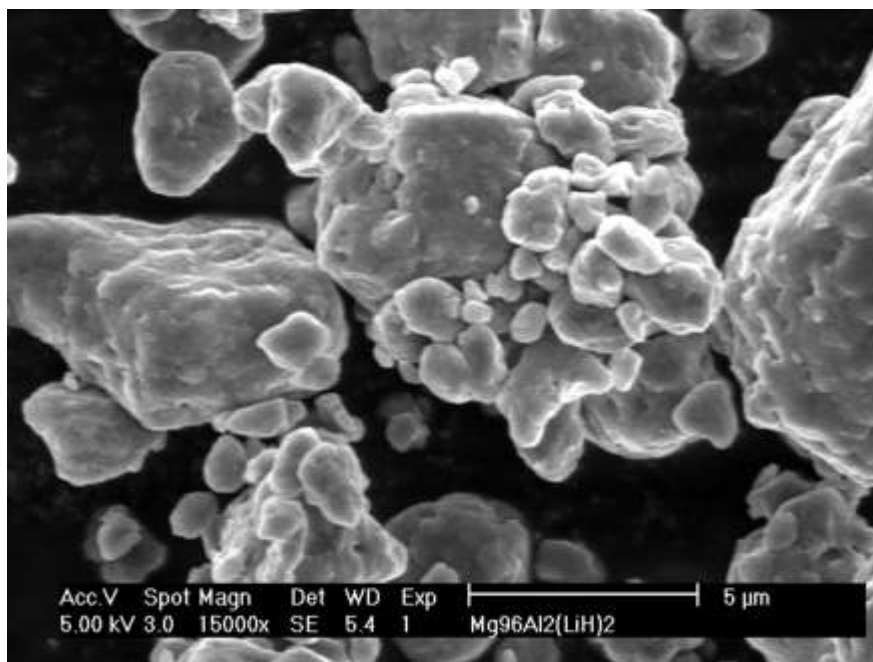


Figure 2. SEM micrograph of as-milled and air-exposed $\text{Mg}_{96}\text{Al}_2(\text{LiH})_2$.



3.2 Hydriding and Dehydriding Experiments

Figure 3 presents the $\text{Mg}_{98}(\text{LiH})_2$ cycling behavior at 350°C as representative of all our tested materials. The hydrogenation at the first cycle was slow and incomplete. As cycling proceeded the hydrogen uptake and hydriding/dehydriding kinetics were improved. Figure 4a presents the first 60 min of the absorption part of the third hydriding/ dehydriding treatment applied to all the mechanically milled powders at 350°C . The pressure increase up to 30 bar is also plotted (grey line). Results for as-milled Mg powders are included for comparison. Mg absorbed about 5.0 wt. % H_2 in 60 min and 5.1 wt. % at the end of experiment; i.e. the smaller value of hydrogen uptake of all the studied alloys. The $\text{Mg}_{98}(\text{LiH})_2$ and $\text{Mg}_{96}(\text{LiH})_4$ mixtures present the fastest kinetics, with a maximum hydrogen uptake of about 5.5 wt. %. In both materials the hydriding reaction is completed in 24 minutes. The $\text{Mg}_{96}\text{Al}_2(\text{LiH})_2$ mixture also showed good hydriding kinetics and good hydrogen uptake. This mixture completed the hydrogen uptake in 36 minutes; it absorbed 6.3 wt.% H_2 . Among the ternary alloys, the $\text{Mg}_{96}\text{Ag}_2(\text{LiH})_2$ mixture presented the slowest hydriding kinetics, even slower than Mg. After 63 minutes, time to complete the hydrogen uptake, $\text{Mg}_{96}\text{Ag}_2(\text{LiH})_2$ stored 5.8 wt.% of H_2 . $\text{Mg}_{96}\text{Zn}_2(\text{LiH})_2$ presented kinetics similar to Mg; after 45 minutes at the hydriding conditions it absorbed 5.2 wt.% as maximum amount of H_2 . $\text{Mg}_{96}\text{Y}_2(\text{LiH})_2$ powders presented good kinetics, the reaction is essentially completed in 27 minutes (5.3 wt.% H_2) and the maximum amount of 5.6 wt.% at the end of experiment. Table II condenses the hydriding characteristics of all the materials tested in the present work. These values are reported at the time of reaching 80% of the maximum hydrogen uptake ($\alpha=0.8$, where α is the transformed fraction, i.e. the ratio between the current hydrogen uptake and the final hydrogen uptake) and at the end of experiment (140 minutes).

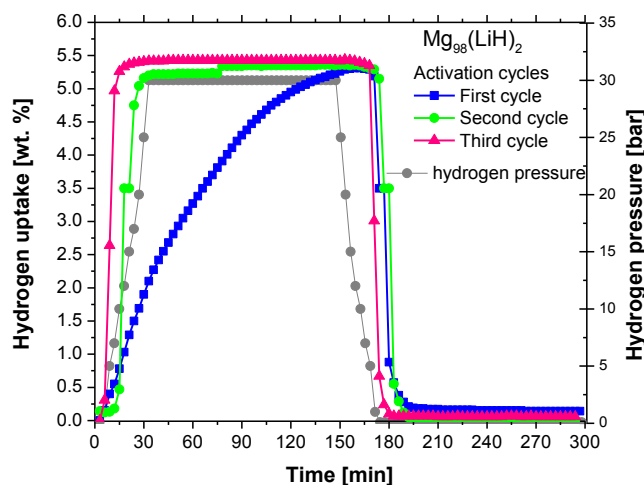


Figure 3. $\text{Mg}_{98}(\text{LiH})_2$ cycling behavior at 350°C .



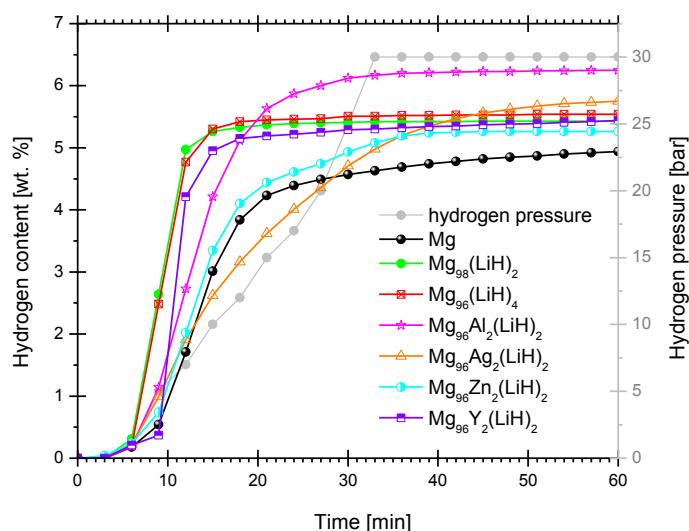


Figure 4a. Hydriding stage at 350°C in the mechanically alloyed powders and pure Mg.

Table II. Summary of hydriding characteristics at 350 and 300 °C. In parenthesis, values from the PCI curves.

Material	350°C / 30 bar		300°C / 30 bar	
	t_{sat} [min] *	Hydrogen content [wt.%] (theoretical; max [†] ; PCI)	t_{sat} [min]*	Hydrogen content [wt.%] (max [†] ; PCI)
Mg ₉₈ (LiH) ₂	11	7.55; 5.4; 5.3	13	5.3; 5.3
Mg ₉₆ (LiH) ₄	12	7.51; 5.6; 5.5	15	5.4; 5.3
Mg ₉₆ Al ₂ (LiH) ₂	18	7.40; 6.3; 6.0	21	6.1; 6.0
Mg ₉₆ Ag ₂ (LiH) ₂	30	6.96; 5.8; 5.5	28	5.2; 5.2
Mg ₉₆ Zn ₂ (LiH) ₂	19	7.18; 5.3; 5.0	36	5.0; 4.9
Mg ₉₆ Y ₂ (LiH) ₂	13	7.06; 5.6; 5.8	24	5.6; 4.8
Mg	20	7.60; 5.1; 4.9	23	5.1; 5.1

* $\alpha = 0.8$ of reaction yield

[†] at 140 min.

The corresponding hydriding processes at 300°C and 30 bar are presented in Fig. 4b (first 60 minutes). At this temperature, Mg₉₈(LiH)₂ and Mg₉₆(LiH)₄ had the fastest kinetics, completing the reaction in 30 minutes. The Mg₉₆Al₂(LiH)₂ mixture showed again the highest hydrogen uptake (6.1 wt.%), completed in 39 minutes. Mg₉₈Ag₂(LiH)₂ and Mg₉₆Zn₂(LiH)₂ showed the slowest hydriding kinetics, even slower than Mg. The hydriding reactions in these materials were completed in 105 and 129 minutes, respectively. Mg₉₆Y₂(LiH)₂ and Mg presented similar slower kinetics and hydrogen uptake (about 57 minutes to



saturate; 5.3 wt.% and 5.0 wt.%, respectively). Table II summarizes the features of the hydriding processes displayed in Fig. 4b.

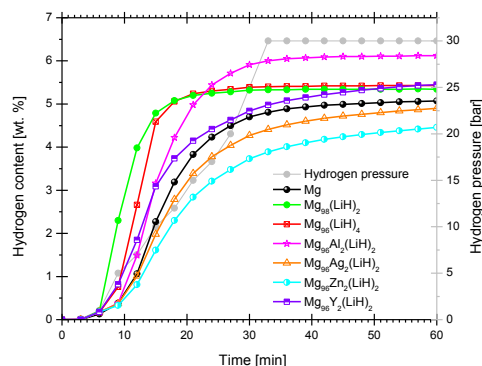


Figure 4b. Hydriding stage at 300°C in the mechanically alloyed powders and pure Mg.

Fig. 5a presents the results of the dehydriding experiments at 350°C. It should be noted that the thermogravimetric equipment used in our experiments was programmed with steps of small pressure changes; large changes in pressure could lead to disturbances. Therefore, the initial time for this stage was taken when the pressure was still 30 bar (grey line); actually, the dehydriding reaction started at about 5 bar for $\text{Mg}_{98}(\text{LiH})_2$ and $\text{Mg}_{96}(\text{LiH})_4$ (18 minutes) and at about 0.1 bar for the ternary alloys (24 minutes). The times for completion of the dehydriding stage at 350 °C are collected in Table III. The values are reported as “effective” values, by taking time zero as the minute 18 (5 bar) for the binary materials and 24 (0.1 bar) for the ternary materials, i.e., the actual pressures at which the dehydriding stage started. $\text{Mg}_{98}(\text{LiH})_2$ and $\text{Mg}_{96}(\text{LiH})_4$ presented a clear improvement on dehydriding kinetics compared with Mg. The reaction is completed in a few minutes for the binary alloys. With some minor differences, the dehydriding kinetics of the Al- and Ag-containing ternary alloys followed the same behavior than Mg. Some hydrogen content (< 0.4 wt.%) seem to remain in some of the alloys according to the curves in Fig. 5a, but this amount may be within the accuracy (zero level) of the testing procedure. The Zn- and Y-containing ternary alloys showed a slight kinetic improvement compared to Mg.

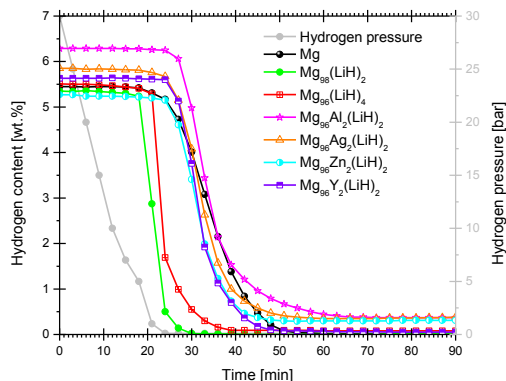


Figure 5a. De-hydrating stage at 350°C in the mechanically alloyed powders and pure Mg.

Table III. Summary of dehydrating characteristics at 350 and 300 °C.

Material	350°C / 0.1 bar		300°C / 0.1 bar	
	t_{end} [min]* χ	H remaining after 140 min [wt.%]	t_{end} [min]* χ	H remaining after 140 min [wt.%]
Mg ₉₈ (LiH) ₂	5	0	20	0.2
Mg ₉₆ (LiH) ₄	9	0	40	0.3
Mg ₉₆ Al ₂ (LiH) ₂	18	0.4	116	3.0
Mg ₉₆ Ag ₂ (LiH) ₂	16	0.4	>116	2.0
Mg ₉₆ Zn ₂ (LiH) ₂	13	0.3	>116	2.4
Mg ₉₆ Y ₂ (LiH) ₂	12	0	57	0.3
Mg	17	0	>116	4.3

* $\alpha = 0.8$ of reaction yield

χ Effective time (registered time minus the beginning time of reaction); 18 minutes for Mg₉₈(LiH)₂ and Mg₉₆(LiH)₄; and 24 minutes for Mg and ternary alloys.

Finally, the kinetics of dehydrating at 300 °C are shown in Fig. 5b. The same correction for an “effective” time is considered in this case for the actual pressures at which the dehydrating reactions began. Here again, the process occurs faster in the Mg₉₈(LiH)₂ and Mg₉₆(LiH)₄ powders (36 and 60 min to completion, respectively; effective time), followed by the Mg₉₆Y₂(LiH)₂ powders (~ 87 min). The remaining alloys did not complete the dehydrating stage at this temperature within the 2.5 hours that the experiments were run. However, it can be seen from Fig. 5a and 5b that the dehydrating kinetics were rather similar in the Mg₉₆Zn₂(LiH)₂ and Mg₉₆Ag₂(LiH)₂ powders. In turn, the Mg₉₆Al₂(LiH)₂ and Mg samples exhibited the slowest kinetic behavior. Table III summarizes the features of the dehydrating processes displayed in Figs. 4b and 5b. Hydriding/ dehydrating and PCI details of Mg₉₈(LiH)₂ and Mg₉₈(LiH)₂ are available in the supplementary file.

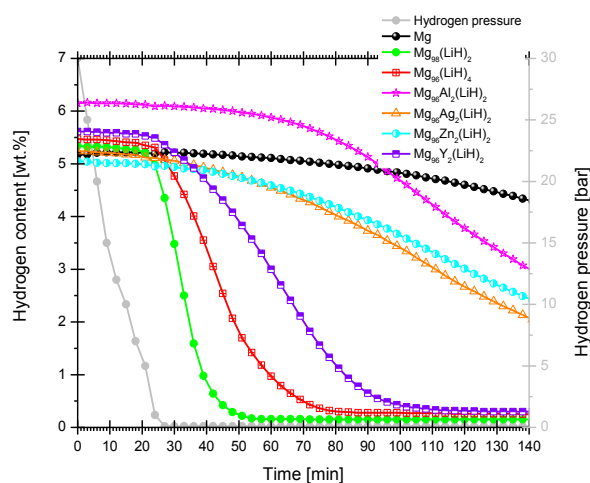


Figure 5b. De-hydrating stage at 300°C in the mechanically alloyed powders and pure Mg.



Due to time-constraining conditions, the PCI curves were not taken strictly at equilibrium conditions; hereafter, these curves are called quasi-PCI curves. The quasi-PCI curves determined at 350 °C are presented in Fig. 6. The upper frame of Fig. 6 displays the quasi-PCI curves of Mg, $\text{Mg}_{98}(\text{LiH})_2$ and $\text{Mg}_{96}(\text{LiH})_4$. The lower frame presents the ternary alloys quasi-PCI curves. The hydriding curves presented plateaus at similar pressures (~ 8 bar) for all the alloyed powders, whereas for Mg the plateau was not well defined; however, the middle point at the semi-plateau is located about 16 bar. The dehydriding quasi-PCI curves at 350° seem to be established under conditions close to equilibrium; in this case, the plateau pressures vary randomly with alloy composition in the range from approximately 2 bar to 4 bar, with the exception of Mg, for which the plateau pressure is about 0.7 bar. From Fig. 6 it can be observed that alloying with Li induced a reduction in the hydriding/ dehydriding hysteresis compared with Mg. In turn, Al, Ag Zn and Y alloying did not introduce further changes. The reduction of hydriding quasi-plateau pressure and the increase of the dehydriding quasi-plateau pressure upon alloying is a change in the correct direction to improve the hydriding/ dehydriding properties of these air-exposed materials.

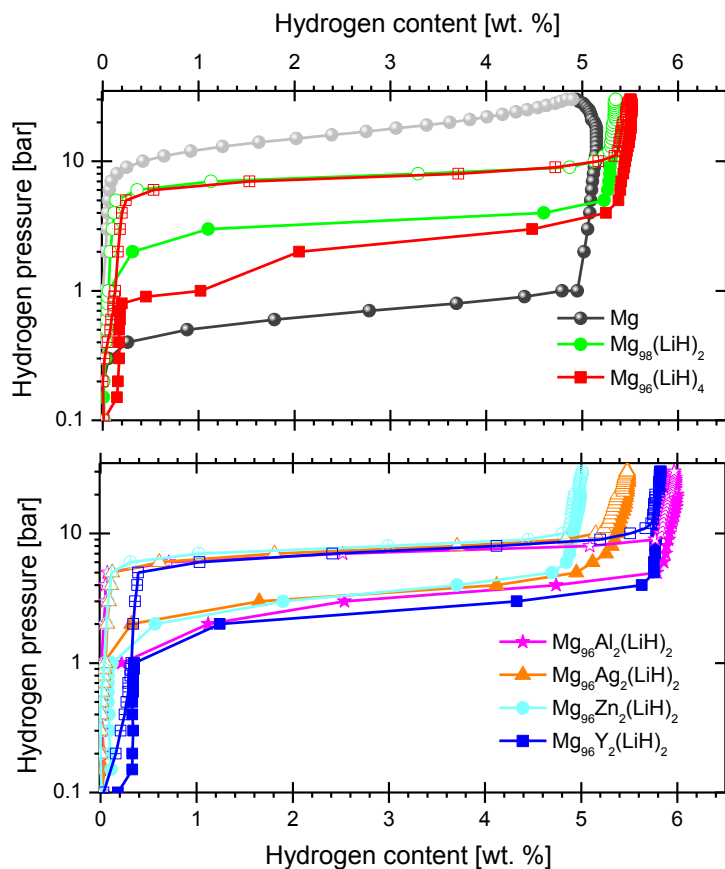


Figure 6. PCI curves determined at 350 °C. Open dots: hydriding. Closed dots: dehydriding.



3.3 XRD and SEM Characterization of Hydrided Powders

Figure 7 presents the XRD patterns from powder mixtures which underwent a final hydriding treatment at 350 °C and 30 bar after the determination of the corresponding quasi-PCI curves. As observed in a number of previous studies [22, 23], the XRD patterns presented a broad peak at the 2 θ position expected for the main reflection from MgO. The Rietveld-estimated crystal size of MgO is about 4 - 7 nm. Table IV presents the composition estimated by Rietveld refinement. The main components are MgH₂ and MgO; the remaining components are elemental Mg, and Fe. Table IV also collects the MgH₂ unit cell parameters and crystallite size obtained from the Rietveld refinement of the XRD data. No correlation of the cell parameters with the alloy components was found. Still, the samples Mg₉₆Al₂(LiH)₂ and, unexpectedly, Mg₉₆Zn₂(LiH)₂ retain the smallest MgH₂ unit cell size. The MgH₂ phase presented a sensible increase of the crystallite size compared with the initial Mg crystallite size in all samples. The Mg₉₈(LiH)₂ and Mg₉₆(LiH)₄ samples have the smallest crystallite sizes. This corresponds also with the quickest de-hydriding kinetics.

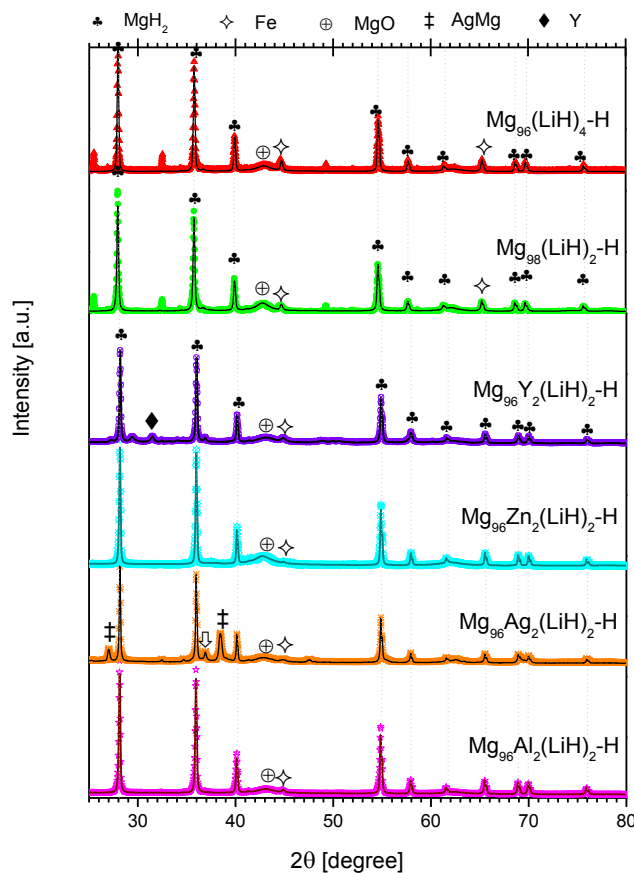


Figure 7. XRD patterns of hydrided powders at 350°C and 30 bar hydrogen pressure. Dots: experimental patterns. Line: refined patterns.



Table IV. Unit cell parameters and crystallite size of hydrided materials at 350°C and 30 bar H₂. Data estimated from XRD refinement.

Hydrided Material	Composition [wt. %]	MgH ₂ unit cell [Å] ICSD-161962 a=b= 4.5140 c= 2.9920	MgH ₂ crystallite size [nm]	MgO crystallite size [nm]
Mg	Mg: 21.0 ± 1.0 MgH ₂ : 60.1 ± 1.2 MgO: 18.9 ± 0.7	a=b= 4.5215 ± 4.2 x 10 ⁻⁴ c= 3.0233 ± 3.5 x 10 ⁻⁴	57.3 ± 6.2	5.6 ± 0.2
Mg ₉₈ (LiH) ₂	Mg: 0.8 ± 0.1 MgH ₂ : 61.4 ± 3.0 MgO: 36.7 ± 1.0 Fe: 1.0 ± 0.1	a=b= 4.5223 ± 4.6 x 10 ⁻⁴ c= 3.0244 ± 3.4 x 10 ⁻⁴	131.7 ± 4.9	7.1 ± 0.2
Mg ₉₆ (LiH) ₄	Mg: 0.8 ± 0.1 MgH ₂ : 67.9 ± 1.0 MgO: 29.2 ± 0.8 Fe: 2.0 ± 0.1	a=b= 4.5217 ± 2.9 x 10 ⁻⁴ c= 3.0241 ± 2.4 x 10 ⁻⁴	129.3 ± 4.3	5.9 ± 0.2
Mg ₉₆ Al ₂ (LiH) ₂	MgH ₂ : 72.9 ± 1.0 MgO: 26.4 ± 0.5 Fe: 0.6 ± 0.1	a=b=4.5182 ± 6.8 x 10 ⁻⁴ c= 3.0219 ± 4.8 x 10 ⁻⁴	191.4 ± 17.9	5.1 ± 0.1
Mg ₉₆ Ag ₂ (LiH) ₂	Mg: 5.0 ± 0.3 MgH ₂ : 54.9 ± 1.0 MgO: 34.8 ± 1.3 MgAg: 5.1 ± 0.1 Fe: 1.0 ± 0.1	a=b= 4.5221 ± 3.1x 10 ⁻⁴ c= 3.0241± 2.3 x 10 ⁻⁴	217.9 ± 12.1	4.6 ± 0.2
Mg ₉₆ Zn ₂ (LiH) ₂	MgH ₂ : 53.0 ± 1.0 MgO: 45.2 ± 0.9 Zn: 1.6 ± 0.1 Fe: 0.2 ± 0.05	a=b= 4.5178 ± 3.6 x 10 ⁻⁴ c= 3.0217 ± 2.5 x 10 ⁻⁴	258.4 ± 16.9	4.1 ± 0.1
Mg ₉₆ Y ₂ (LiH) ₂	MgH ₂ : 67.3 ± 1.0 MgO: 28.8 ± 0.9 Y: 1.7 ± 0.8 Fe: 2.1 ± 0.1	a=b= 4.5196 ± 2.9 x 10 ⁻⁴ c= 3.0228 ± 2.1 x 10 ⁻⁴	196.8 ± 8.8	6.8 ± 0.3



A representative SEM picture of the hydrided materials is presented in Figure 8. More images are available as supporting info. The surface of the hydrided materials presented protuberances. This has been related with the nucleation and growing of MgH_2 over Mg particles [24].

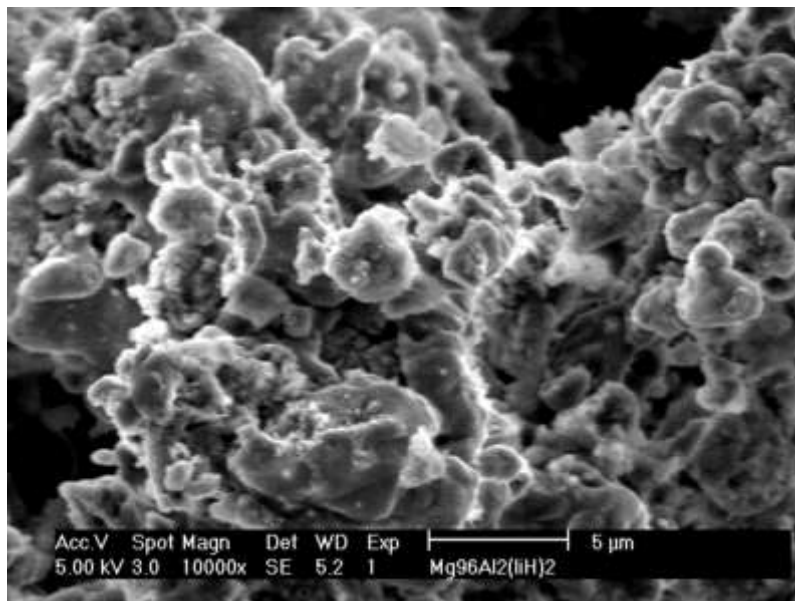


Figure 8. SEM micrograph of hydrided $\text{Mg}_{96}\text{Al}_2(\text{LiH})_2$ at 350°C and 30 bar hydrogen pressure.

4. Discussion

4.1 LiH effect on Hydrogen Storage Properties

The results presented in this paper have indicated a significant accelerating effect of the kinetics of hydriding/ dehydriding reactions in oxide-covered Mg-base alloys by the addition of a small amount of LiH. Interestingly, the addition of 2 mole% LiH had a significantly higher accelerating effect than a larger addition of 4 mole%. In terms of the times to reach uptake saturation and complete dehydriding (Tables II and III); the kinetics in the $\text{Mg}_{98}(\text{LiH})_2$ mixture improved by a factor of 2 in hydriding, and at least by 3 in dehydriding processes in comparison to as-milled Mg. Smith et al. [25] in a recent theoretical study on the substitution of Li^+ for Mg^{2+} in MgH_2 indicates that Li doping may enhance the hydrogen diffusion but only to a limited extent determined by an optimal dopant concentration. Liang et al. [26] and Huot et al. [27] previously reported some hydrogen storage properties of Mg-Li alloyed powders produced by mechanical alloying. In the work of Liang et al., the amount of Li was 10 at.%, but vanadium and graphite were also added in the amounts of 2.5 at.% and 2 wt.%, respectively [26]. Despite the expected catalytic activity of vanadium in this material, the reported kinetics of hydriding/ dehydriding processes at 350 °C are comparable to what is shown for our Mg-LiH alloys in Figs. 4a and 5a. On the other hand, the final materials prepared by Huot et al. [27] by lixiviation of Li from a mechanically alloyed Mg- 28 at.% Li



powder mixture, probably contained a small amount of Li (no final chemical analysis was given by the authors). In this case also the kinetics of hydriding/ dehydriding are close to those found in our work, at the same temperature of 350 °C. These authors suggested that the improved kinetics in their materials (as compared to Mg) was mainly the result of a much larger specific surface area in the lixiviated products. Taken together, the work of Liang et al. and Huot et al. seem to be consistent with the results of our own in that a small addition of Li induces considerably beneficial kinetics effects in the hydrogen storage properties of Mg powders.

The mechanisms by which Li influences the hydrogen storage characteristics of Mg powders may be complex and are open to debate. In a recent paper, Palacios et al. [28] had shown that a mixed hydride of the composition $\text{Mg}_{15}\text{LiH}_{32}$ has a lower thermodynamic stability than pure MgH_2 ($\Delta H_f = -58.3 \text{ kJ}\cdot\text{mol}^{-1}$ and $\Delta H_f = -71.7 \text{ kJ}\cdot\text{mol}^{-1}$ respectively); this, by itself, it is usually taken as a good indication of lower decomposition temperatures for the hydride phase [29], or conversely, faster reaction kinetics at a given temperature. A destabilizing effect had been observed in other Li-containing hydrogen storage materials such as $\text{LiBH}_4/\text{MgH}_2$ [30]. Nonetheless, the full explanation of the hydriding/dehydriding kinetics of our Mg-LiH powders is not solely based on the thermodynamic stability of the different hydrides, but also in structural factors.

4.2 Effect of M (M = Al, Ag, Zn and Y) Additions on Hydrogen Storage Properties

It is clear from the kinetics and PCI data (Figs. 4 to 6) that the addition of Ag, Zn and Y in the ternary powder mixtures did not represent any benefit to the hydrogen storage properties over those obtained by the addition of LiH alone. On the contrary, in these cases the ternary addition resulted in unfavorable properties compared to those shown by as-milled Mg, our reference material. Only the addition of Al seems to have improved the hydrogen uptake, but not the hydriding/dehydriding kinetics. Surprisingly, despite the large volume of literature dedicated to the hydrogen storage properties of Mg-based alloys, we have not found reports involving dilute, binary alloys of Al, Ag, Zn or Y in magnesium in which a consistent comparison of their hydriding/dehydriding properties with those of Mg was accomplished. A semi-quantitative comparison of mechanically milled Mg powders with mechanically alloyed Mg-M mixtures (M = Al, Ag, Zn and Y), having a nominal content of 2 at.% M, was presented recently by Palacios et al. [20]. According to their results, the additions of these elements had the effect of reducing the production of MgH_2 in basically all the alloyed powders and hydriding conditions

4.3 Effect of MgO on Hydrogen Storage Properties

An amorphous layer or islands of MgO could be formed during the air-exposure step after ball milling, which would become crystalline when being subjected to higher temperatures, as suggested by the XRD of as-milled and hydrided materials. Shih et al. [31] proposed the mechanism of MgO formation over Mg as the following successive steps: oxygen chemisorption on the magnesium surface, formation and coalescence of oxide islands and oxide thickening. It was believed for a long time that the formation of oxide layers prevented at all further hydrogen uptake in Mg materials [32]. However, it was recently reported that the addition up to 10 wt.% of MgO to MgH_2 can reduce the dehydriding temperature to 262°C [33]. Barkhordarian et al demonstrated the potential use of metal oxides as suitable catalyst for hydrogen storage purposes [34]. In both reports, the metal oxides were milled together with the MgH_2 . Borgschulte et al. [35] demonstrated that a surface layer of MgO is able to recombine atomic hydrogen. Friedrichs et al. performed a hydrogen desorption kinetics study of air- exposed Mg catalyzed with 2 mol % of Nb_2O_5 [36]. In that study; in the sample exposed to air for 24 hours, the hydrided Mg was able to



desorb about 3 wt.% hydrogen at 300°C and 0.001bar in 30 min. The 1 hour air-exposed sample was able to desorb about 4 wt. % under the same conditions. The present work demonstrates that 5.0 to 6.2 wt. % hydrogen storage is still feasible after deliberate air-exposure for 12 hours our Mg alloys. Meanwhile, the amount of MgO formed is apparently between 18.9 and 45.2 wt%. Similar MgO weight fractions had been frequently determined in a number of studies [20, 37]. Let us remark that this drop in storage capacity is a frequent observation in the literature on Mg-based alloys [38, 39, 40, 41]. A second common observation in such cases is the existence of a considerable amount of “disordered” magnesium oxide [39, 40, 42], evidently as a consequence of the high affinity of magnesium for oxygen and the large amount of “fresh” (reactive) surface area found in powders right after their production and/or after being subjected to a dehydriding treatment.

Two phenomenon have been proposed for explaining the observed dehydriding reactions at MgO covered MgH₂ [35]: (1) that the inactive MgO forms nano or micro-cracks, channels or pathways [31, 36], exposing fresh and active Mg/ MgH₂ surfaces; and (2) that the MgO formed on top of MgH₂ is indeed active by the formation of oxygen vacancies during hydrogen exposure and heating [36]. The SEM images (at the micrometer observation size range) do not reveal cracks or fissures on the surface of the powder particles, but the agglomerates look smaller in size. The cycling behavior presented in Figure 3 (common to all our samples), indicates the difficulty of performing the first hydriding reaction. This is consistent with the existence of an obstructive layer. Shih et al. [31] also proposed that the different thermal expansion coefficients of Mg and MgO could lead to cracks in the oxide film. This can explain in part the improvement in the hydriding/dehydriding kinetics after cycling.

5. Conclusions

Mg₉₈(LiH)₂, Mg₉₆(LiH)₄ and Mg₉₆M₂(LiH)₂ (M=Al, Ag, Zn and Y) alloys were produced by mechanical alloying and deliberately air-exposed after milling. Despite the formation of MgO, this alloy production technique is still suitable for hydrogen storage materials and has the potential to reduce the cost of using a high purity protective atmosphere during alloy fabrication and handling. The addition of Al, Ag, Zn or Y to Mg₉₆(LiH)₄ does not improve the kinetics of hydriding/ dehydriding. However, there is some improvement with respect to milled, nanocrystalline Mg. A special case is the Mg₉₆Al₂(LiH)₂ alloy in which the quantity of hydrogen stored increased as compared to Mg₉₆(LiH)₄ and Mg milled under the same conditions. The present results of the air-exposed Mg-based alloys would be useful in the design and practical production of new ternary and quaternary materials for hydrogen storage.

Acknowledgements

KSA and JGCM thank CINVESTAV for technical support. KSA thanks DGECI-UNAM for a mobility grant.

6. References

- [1] R. Barbosa, J. Andaverde, B. Escobar, U. Cano, Stochastic reconstruction and a scaling method to determine effective transport coefficients of a PEMFC catalyst layer. J. Power Sources 2011; 196: 1248–1257
- [2] A. J. Bard and L. R. Faulkner, Electrochemical Methods, Fundamentals and Applications, 2nd ed., John Wiley & Sons, Inc., N. Y., 2000.



-
- [1] R. C. Jr Bowman, B. Fultz, Metallic Hydrides I: Hydrogen Storage and Other Gas-Phase Applications. MRS Bulletin 2002; 27: 688-693.
- [2] L. Schlapbach, A. Züttel, Hydrogen-storage materials for mobile applications. Nature 2001; 414: 353-358.
- [3] M. Felderhoff, B. Bogdanović, High Temperature Metal Hydrides as Heat Storage Materials for Solar and Related Applications. Int. J. Mol. Sci. 2009; 10: 325-344.
- [4] Y. Oumellal, A. Rougier, G.A. Nazri, J.M. Tarascon, L. Aymard, Metal hydrides for lithium-ion batteries. Nature Materials 2008; 7: 916-921.
- [5] M. Ramzan, S. Lebegue, R. Ahuja, Transition metal doped MgH_2 : A material to potentially combine fuel-cell and battery technologies. Int. J. of Hydrogen Energy 2010; 35: 10373-10376.
- [6] J. Huot, G. Liang, R. Schulz, Mechanically alloyed metal hydride systems. Appl. Phys. A. 2001; 72: 187-195.
- [7] K. H. J. Buschow, P. C. P. Bouten, A. R. Miedema, Hydrides formed from intermetallic compounds of two transition metals: a special class of ternary alloys. Rep. Prog. Phys. 1982; 45: 937-1039.
- [8] N. Hanada, T. Ichikawa, S.I. Orimo, H. Fujii, Correlation between hydrogen storage properties and structural characteristics in mechanically milled magnesium hydride MgH_2 . Journal of Alloys and Compounds 2004; 366: 269-273.
- [9] S. Er, D. Tiwari, G. A. Wijs, G. Brocks, Tunable hydrogen storage in magnesium-transition metal compounds: First-principles calculations. Physical Review B. 2009; 79: 024105-8.
- [10] F.P. Luo, H. Wang, L. Z. Ouyang, M. Q. Zeng, J. W. Liua, M. Zhua, Enhanced reversible hydrogen storage properties of a Mg-In-Y ternary solid solution. Int. J. of Hydrogen Energy 2013; 38: 10912-10918.
- [11] H. Shao, M. Felderhoff, F. Schuth, C. Weidenthaler, Nanostructured Ti-catalyzed MgH_2 for hydrogen storage. Nanotechnology 2011; 22: 235401-7.
- [12] L. Baum, M. Meyer, L. Mendoza-Zélis, Hydrogen storage properties of the Mg/Fe system. Physica B: Condensed Matter 2007; 389: 189-192.
- [13] Y. Song, Z. X. Guo, R. Yang. Influence of selected alloying elements on the stability of magnesium dihydride for hydrogen storage applications: A first-principles investigation. Physical Review B 2004; 69: 094205-11.
- [14] K. Miwa, A. Fukumo, First-principles study on 3d transition-metal dihydrides. Physical Review B. 2002; 65: 155114-7.
- [15] K. Nakatsuka, M. Yoshino, H. Yukawa, M. Morinaga, Roles of the hydride forming and non-forming elements in hydrogen storage alloys. J. Alloys and Compounds. 1999; 293-295: 222-226.
- [16] H. Yukawa, T. Matsumura, M. Morinaga, Chemical bond state and hydride stability of hydrogen storage alloys. J. Alloys and Compounds. 1999; 293-295: 227-230.
- [17] H. Smithson, C.A. Marianetti, D. Morgan, A. Van der Ven, A. Predith, G. Ceder, First-principles study of the stability and electronic structure of metal hydrides. Physical Review B. 2002; 66: 144107-10.
- [18] W. Grochala, P.P. Edwards, Chemical tuning of the thermal decomposition temperature of inorganic hydrides: Computational aspects. J. Alloys and Compounds. 2005; 404-406: 31-34.
- [19] N. Hanada, T. Ichikawa, S. Hino, H. Fujii, Remarkable improvement of hydrogen sorption kinetics in magnesium catalyzed with Nb_2O_5 . Journal of Alloys and Compounds 2006; 420: 46-49.
- [20] A. F. Palacios-Lazcano, J. L. Luna-Sánchez, F. Cruz-Gandarilla, J. G. Cabañas-Moreno, Hydrogen storage in nanostructures Mg-Base alloys. J. Nano Research 2009; 5: 213-221.
- [21] L. Lutterotti, Maud: a Rietveld analysis program designed for the internet and experiment integration. Acta Cryst. 2000; A56 (Supplement) s54.
- [22] J. Huot, G. Liang, S. Boily, A. Van Neste, R. Schulz, Structural study and hydrogen sorption kinetics of ball-milled magnesium hydride. J. Alloys and Compounds 1999; 293-295: 495-500.
- [23] R. A. Varin, S. Lia, A. Calka, Environmental degradation by hydrolysis of nanostructured -MgH_2 hydride synthesized by controlled reactive mechanical milling (CRMM) of Mg. J. Alloys and Compounds 2004; 376: 222-231.
- [24] L. Mooij, B. Dam, Nucleation and growth mechanisms of nanomagnesium hydride from the hydrogen sorption kinetics. Phys. Chem. Chem. Phys. 2013; 15: 11501-11510.
- [25] K. C. Smith, T. S. Fisher, U. V. Waghmare, R. Grau-Crespo, Dopant-vacancy binding effects in Li-doped magnesium hydride. Physical Review B 2010; 82: 134109-9.
- [26] G. Liang, Synthesis and hydrogen storage properties of Mg-based alloys. J. Alloys and Compounds 2004; 370: 123-128.



- [27] J. Huot, S. Bouaricha, S. Boily, J. P. Dodelet, D. Guay, R. Schulz, Increase of specific surface area of metal hydrides by lixiviation. *J. Alloys and Compounds*, 1998; 266:307–310.
- [28] A. F. Palacios-Lazcano, H. Yukawa, M. Morinaga, J. G. Cabañas-Moreno, Stability of mixed magnesium hydrides (Mg-M)H₂ (M = Al, Ag, Ga, Li, Sc, Y, Zn) estimated by density functional theory. (2014) Submitted to Transactions JIM.
- [29] W. Grochala, P. Edwards, Thermal decomposition of the non-interstitial hydrides for the storage and production of hydrogen. *Chem. Rev.* 2004; 104:1283-1315.
- [30] T. E. C. Price, D. M. Grant, D. Weston, T. Hansen, L. M. Arnbjerg, D. B. Ravnsbæk, T. R. Jensen, G. S. Walker, The effect of H₂ partial pressure on the reaction progression and reversibility of Lithium-containing multicomponent destabilized hydrogen storage systems. *J. Am. Chem. Soc.* 2011; 133: 13534-13538.
- [31] T. S. Shih, Y. B. Liu, P. S. Wei, Oxide films on magnesium alloys. *Materials Chemistry and Physics* 2007; 104: 497-504.
- [32] C. W. Ostenfeld, M. Johansson, I. Chorkendorff, Hydrogenation properties of catalyzed and non-catalyzed magnesium films. *Surf Sci.* 2007; 601: 1862-1869.
- [33] J. R. Ares-Fernández, K. F. Aguey-Zinsou, Superior MgH₂ kinetics with MgO addition: a tribological effect. *Catalysts* 2012; 2 :330-343.
- [34] G. Barkhordarian, T. Klassen, R. Bormann, Fast hydrogen sorption kinetics of nanocrystalline Mg using Nb₂O₅ as catalyst. *Scripta Materialia* 2003; 49: 213–217.
- [35] A. Borgschulte, M. Biemann, A. Züttel, G. Barkhordarian, M. Dornheim, R. Bormann, Hydrogen dissociation on oxide covered MgH₂ by catalytically active vacancies. *Appl. Surf. Sci.* 2008; 254: 2377–2384.
- [36] O. Friedrichs, J. C. Sánchez-López, C. López-Cartes, T. Klassen, R. Bormann, A. Fernández, Nb₂O₅ “Pathway Effect” on Hydrogen Sorption in Mg. *J. Phys. Chem. B* 2006; 110: 7845-7850.
- [37] A. Montone, J. Grbovic, A. Bassetti, L. Mirengi, P. Rotolo, E. Bonetti, L. Pasquini, M. Vittori Antisari, Microstructure, surface properties and hydrating behaviour of Mg–C composites prepared by ball milling with benzene. *Int. J. Hydrogen Energy* 2006; 31: 2088 – 2096.
- [38] O. Gutfleisch, S. Dal Toe, M. Herrich, A. Handstein, A. Pratt, Hydrogen sorption properties of Mg–1 wt.% Ni–0.2 wt.% Pd prepared by reactive milling. *J. Alloys and Compounds* 2005; 404–406: 413–416.
- [39] T. Czujko, R. A. Varin, Ch. Chiu, Z. Wronski, Investigation of the hydrogen desorption properties of Mg + 10 wt.% X (X = V, Y, Zr) submicrocrystalline composites. *J. Alloys and Compounds* 2006; 414: 240–247.
- [40] G. Barkhordarian, T. Klassen, R. Bormann, Kinetic investigation of the effect of milling time on the hydrogen sorption reaction of magnesium catalyzed with different Nb₂O₅ contents. *J. Alloys and Compounds* 2006; 407: 249–255.
- [41] G. Liang, J. Huot, S. Boily, A. Van Neste, R. Schulz, Catalytic effect of transition metals on hydrogen sorption in nanocrystalline ball milled MgH₂–Tm (Tm=Ti, V, Mn, Fe and Ni) systems. *J. Alloys and Compounds* 1999; 292: 247–252.
- [42] A. Révész, D. Fátay, T. Spassov, Hydriding kinetics of ball-milled nanocrystalline MgH₂ powders. *J. Mater. Res.* 2007, 22: 3144-3151.

